京都大学防災研究所年報 第43号 B-1 平成12年4月
Annuals of Disas. Prev. Res. Inst., Kyoto Univ., No. 43 B-1, 2000

Fluidization Behavior of Sands Based on Ring Shear Tests
—— Effects of Grain Size and Fine-Particle Content ——

Gonghui WANG and Kyoji SASSA
Disaster Prevention Research Institute, Kyoto University, Kyoto, Japan

Synopsis

Using a newly developed ring shear apparatus, several sets of undrained ring shear tests were conducted on sands of different grain size and fine-particle content to study the effects of samples on the fluidization behavior within the shear zone. By inserting slices of Toyoura sand with different color into the shear box, the deformation of sands within the shear box was observed after 3-cm of undrained shearing, and it was made clear that localized shearing was formed in both the tests on loose sand and dense sand. Grain size analysis on the samples from the shear zone after the undrained shear tests revealed that grain crushing was initiated in the shear zone. By performing tests on sands of the same density at different stress states, the collapse behavior of loose sands in ring shear tests were examined, and the collapse line was found passing through the origin, and dependent on sample's initial density and grain size. The brittleness index increased with increasing initial normal stress and shear stress. Based on the tests results, the effects of grain size and fine-particle content on the undrained shear behavior were examined. And the results showed that, given their relative densities being the same, when the grain size became finer or fine-particle content became greater, both the undrained peak shear strengths and steady state shear strengths became smaller, meanwhile, the dissipation of generated high pore pressure from the shear zone became slower after the shear box was turned into drained condition.

Keywords: Excess pore pressure; Shear resistance; Ring-shear tests; Sands; Grain Size, Fine-particle content

1. Introduction

The undrained shear behaviour of sand is a knotty problem to civil engineers in dealing with a situation where soil liquefaction may occur. It is closely related to the determining of stress conditions required to trigger liquefaction, and the analyzing of the consequences of liquefied mass in terms of potential deformation.

As well known, liquefaction could be triggered by cyclic loading, such as earthquakes (Seed 1966; Ishihara *et al.*, 1990), or by static effects, such as rainfall (Eckersley, 1985; Adderson and Sitar 1995; Sassa, 1998a), melted snow, etc. (Marui, 1996; Sassa et al, 1997a). Liquefaction of sands due to cyclic loading has received a great deal of attention since the Niigata, Japan, earthquake of 1964 (Yoshimi et al., 1977; Seed 1979; Finn 1981), and the behaviour of sands subjected to undrained cyclic loading has been made relatively clear. In addition, static liquefaction due to monotonic increase of static loading has been studied in recent years (Castro, 1969; Casagrande, 1976; Castro and Poulos, 1977; Poulos, 1981; Poulos et al., 1985), and based on the tremendous results of

mostly triaxial tests, a very appealing concept of ultimate steady state was proposed and widely used in the procedure of analyzing liquefaction susceptibility of a soil in anti-liquefaction design (Vaid and Chern 1983; Poulos et al., 1985; Alarcon-Guzman *et al.* 1988; Kramer and Seed, 1988). The essential criterion of this procedure is that saturated soil with void ratio and effective stress located below the steady state line in the "*e-logp*" diagram is impossible to suffer liquefaction failure.

Nevertheless, recent undrained ring shear tests showed some inconsistent tendency, liquefaction being able to be triggered even in very dense sand due to grain crushing accompanying increasing shear displacement. In the studies of earthquake-triggered-landslides based on ring shear tests, a concept of sliding surface liquefaction was proposed by Sassa to interpret the high mobility of failed landslide mass. Sliding surface liquefaction is a special kind of liquefaction; it differs from the pronounced (mass) liquefaction (Sassa, 1996). Sliding surface liquefaction is a phenomenon that liquefaction only takes place along the sliding surface. With increasing shear displacement, accompanying the grain crushing, pore water pressure builds up gradually, and shear resistance decreases slowly, finally tend to constants respectively. Therefore, Sliding surface liquefaction can take place even in medium or dense soil structure; and it is a localized liquefaction limited in the shear zone both in laboratory test and on the field.

Recently, Sassa and colleagues had carried out tremendous ring shear tests on different samples under different loading conditions (static load and cyclic load) to study the mechanism of sliding surface liquefaction, with emphasis on the relationship between grain crushing susceptibility and pore pressure generation, etc. (Sassa 1996; Sassa *et al.* 1997a, b; Vankov and Sassa 1998; Wang 1998). However, most of these studies were concentrated on the sliding surface liquefaction behavior, i.e., focusing on the undrained behavior of dense and medium dense specimens that exhibit dilative behavior. In this sense, the loose specimen was less studied in ring shear tests. Further more, as has been pointed out, in many cases of liquefaction-induced slope failure, the liquefaction was just limited in the sliding zone (Casagrande 1971; Castro 1992; Sassa et al. 1998; Seed 1968); and some laboratory researches have found that shear bonding could even be formed in very loose sand when subjected to shearing. Nevertheless, compared with the huge number of undrained triaxial tests, the undrained shear behavior of sand in the shear zone is still poorly understood and needs further scrutiny.

On the other hand, investigations into the shear behaviour of granular soils have generally concentrated on clean sands, which contains only relatively small quantities of silt and no clay. But as reported, natural sands often contain significant proportions of both silt and clay (Ishihara, 1985), and silt and silt-clay mixture are more prone to suffer form liquefaction failure with large resulting run-out distance, on the basis of many field observations (Bishop 1973; Eckersley 1990; Georgiannou et al. 1990; Ishihara et al. 1990; Keith Turner & Schuster 1996). However, the undrained shear behaviour of silt and silt-clay mixtures is not very clear. For evaluating the liquefaction potential of this kind of soil, there is no guideline available based on their density, void ratio, plasticity index, standard penetration values, or any other simple soil property. And even more, there is confusion on the influence of clay content, plasticity index, and void ratio, as pointed out by Guo & Prakash (1999). For example, by performing series tests on loose samples prepared with varying percentages of both plastic and nonplastic fines (<74 μ m) and nonplastic fine sand (>74 μ m), Pitman *et al* (1994) found that undrained brittleness decreased as the fines content, for both plastic and nonplastic type, increased; at a fines content of 40% the stress path indicated only strain hardening towards steady state, i.e., no brittleness. Another research carried out by Ovando-Shelley and Perez (1997) had pointed out that within limited range of clay content, the presence of clay increases the potential for generating excess pore pressure during undrained loading, and also reduces strength and stiffness. From these researches, it could be concluded that the undrained shear behavior of silt and silt-clay mixtures is not very clear and needs further extensive scrutiny.

Therefore, in this research, using a newly made ring shear apparatus series tests were conducted on sands with different grain sizes and fine-particle (loess) contents. By performing tests at large range of relative densities and at different initial stress states, the different undrained shear behaviors are examined. Basing on the tests results, the mechanism of fluidization in the shear zone is analyzed.

2. Sample Characteristics

In this study, fine silica sand no. 7 (S7) and no. 8 (S8) are selected as the sample. These silica sands are kinds of sand materials for building use made from silica sandstone by mechanical grinding, comprised of 92-98 percent of subangular to angular quartz, and

Table 1 Properties of employed samples, S7, S8, M10, M20, M30, and loess

Sample	S7	S8	Loess	M10	M20	M30
Mean grain size, D_{50} (mm)	0.13	0.050	0.0185	0.047	0.043	0.040
Effective grain size, D_{10} (mm)	0.074	0.018	0.0012	0.0118	0.0084	0.0057
Uniformity coefficient, U_c	2.1	3.7	19.0	4.6	6.0	8.3
Maximum void ratio, e_{max}	1.23	1.66	-	1.51	1.52	1.56
Minimum void ratio, e_{min}	0.70	0.85	-	0.73	0.73	0.73
Specific gravity, G_s	2.63	2.63	2.72	2.64	2.65	2.66

Note: -: value was not measured.

a little amount of feldspar. The particles ranged from fine sand to silt sizes. To study the influence of fine-particle on liquefaction behaviour, loess was used in this research, too. This loess, which was composed mainly of silt, was collected from a potential landslide at Lishan, Xi'an, China. In the present work, a series of tests was conducted on the mixture of S8 and loess with loess content being 10, 20, and 30 percent, which were termed as M10, M20 and M30, respectively. The grain-size distributions of S7, S8 and loess are shown in Figure 1; and some characteristics of the employed samples are listed in Table 1.

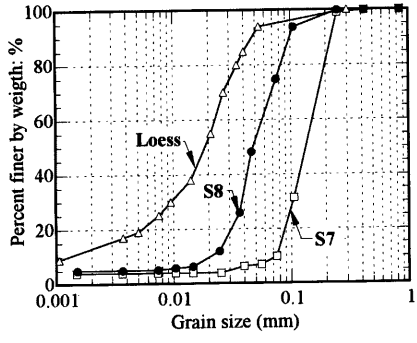

Fig.1 Grain-size distribution of silica sand no. 7, no. 8, and loess.

3. Test Apparatus and Test Procedure

3.1 Ring shear apparatus

Two new sets of almighty intelligent ring shear apparatus (DPRI-Ver.5, DPRI-Ver.6) were developed and improved by Sassa and colleagues to simulate the earthquake-triggered-landslides after the Hyogoken -Nanbu earthquake, 17th January 1995, Japan. A detailed description of these series of undrained ring shear apparatus was given by Sassa (1997). In the present research, DPRI-Ver.6 was employed. A schematic illustration of the apparatus is shown in Figure 2a.

Figure 2b shows the shear mode of sample in ring-shear apparatus briefly. The sample is laterally confined between pairs of upper and lower confining rings, and loaded normally through an annular loading platen connected to an oil piston through load lever. The low half of the shear box is rotary in both directions, driven by a servomotor through transmission system, while the upper part is kept steady with help of two reacting torque arms, with which the shear resistance is measured. When shear failure happened, the annular ring-shaped sample will be sheared on a plane of relative rotary motion, with the lower part rotating along with rotating table.

The most essential design for undrained ring shear apparatus is the construction of undrained shear box. Its design is illustrated as Fig. 2c, an enlarged diagram of the undrained edges and its surroundings, including water-pressure measurement system. Water-leakage proof is made by rolling two slices of "O" rings on the upper loading platen, and pasting rubber edges on the two confining rings of the low rotary pair. Before setting the shear box, the rubber edges are covered with friction coat of Teflon, and daubed with vacuum silicon grease. During test, a certain mount of pressing fore (determined by the possible generation of pore pressure) is applied between the upper pair and rubber edges, and kept constant automatically through a gap control oil piston controlled by a servomotor using the feed back signal obtained from a gap sensor with a resolution of 1/1000 mm. For DPRI-Ver.6, the shear box is 250 mm in inner diameter, 350 mm in outer diameter, and 150 mm in height. Pore pressures are measured by pore pressure transducers, which are connected to the gutter (4×4 mm) along the whole circumference on the inner wall of the outer ring in the upper pair. The gutter is located at 2 mm above the shear surface and covered with two metal filters, with a filter cloth between them.

Two personal computers are set for test controlling and data recording. Testing process is controlled by an operating computer. The test could

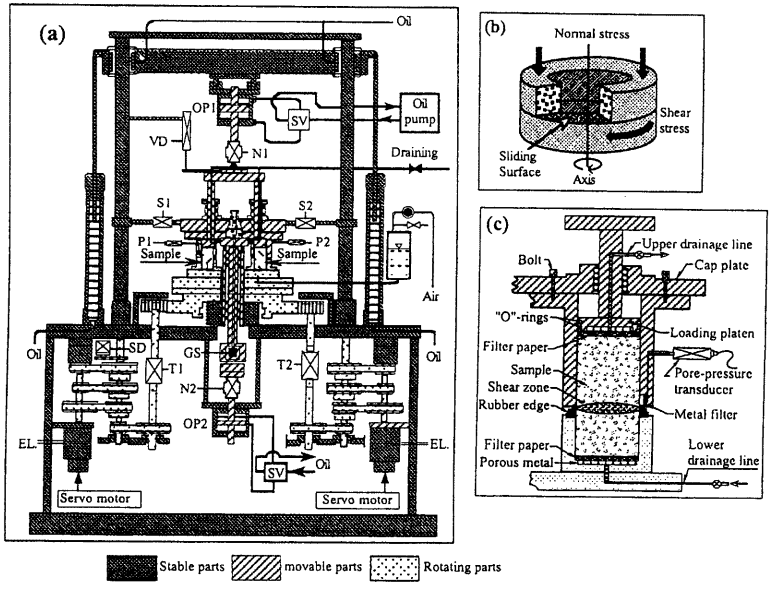

Fig. 2. Ring shear apparatus (DPRI-Ver.6). (a) Schematic diagram; (b) Annular ring-shaped sample; (c) Enlarged diagram of undrained shear box.

be either shear-torque-controlled, or shear-speed-controlled. In the present research, to observe the shear behaviour of soil accompanying the increasing shear stress before failure, shear-torque-controlled method is selected. All the recordings of transducers are recorded automatically, while the graph of effective stress path is being drawn simultaneously by the data-recording computer.

3.2 Test procedure

The samples were made by means of moist placement or dry deposition (Ishihara, 1993), according to different test purposes. For moist placement method, de-aired water was first added to the oven-dried samples to make the initial water content rise up to 5 percent, and then the sand was stirred evenly. After that, the sample was placed into the shear box. To make the sample uniform, while packing, the sample was placed in a series of layers of 3-cm thickness, and then each layer was tamped. For dry deposition method, the oven-dried sample fell into the shear box freely by layers, and each layer was and was not tamped differently to make the initial density different. Sample was saturated with help of carbon dioxide and de-aired water. Considering the possible effects of backpressure on test results, during saturation, back pressure was not applied. In all the tests, saturation degree was checked by using B_D parameter. B_D is a parameter of saturation in the direct shear state, which was proposed by Sassa (1988a), and formulated as:

$$B_D = \Delta u / \Delta \sigma \qquad (1)$$

where Δu and $\Delta \sigma$ are the increment of pore pressure and normal stress, respectively. If $B_D \geqq 0.95$, it shows a full saturation. In this study, all the tests were carried out with $B_D \geqq 0.95$.

All the samples were normally consolidated. After consolidation, undrained shear stresses were subsequently applied at a loading rate of 0.098 kPa/sec. Transducers were scanned at a interval of 1 second before the peak shear strength; after that, the sampling rate was increased to 20 samples/sec. Corresponding to the shear stress control, there are three kinds of rotating gear with final speed of Low (10 mm/sec), Medium (32.3 cm/sec) and High (2.25 m/sec). In this study, the Low gear was selected.

To observe the generation of pore pressure accompanying the shear displacement, the samples were sheared to steady state, i.e., the pore pressure

and shear resistance did not change further more.

4. Experimental Results

Since it is impossible to present the results of all the tests that were carried out, here some typical results were selected to present the undrained shear behavior in different test conditions, with emphasis on examining the effects of initial relative density, initial stress state, grain size, and fine-particles on the undrained shear behavior.

4.1 Effects of initial relative density on the undrained shear behaviors

It has been pointed out that the initial relative density plays an important role in the undrained shear behavior (Castro 1969, Ishihara 1993). To make a good understanding of the undrained shear behavior of sand in ring shear tests, tests results were divided into two series according to their effective stress paths, to interpret their typical characteristics. One series is the tests on loose sand showing a typical effective stress path of mass liquefaction, with quick strain softening process that resulted in collapse failure; the other series is the tests on medium to dense sand showing the effective stress path of sliding surface liquefaction, with a process from strain softening to strain rehardening, and finally followed by liquefaction caused by grain crushing. Here, test results were presented to show their unique characteristics.

(1) Ring shear tests on loose sand

The results of one test on loose sand S8 showing mass liquefaction behaviour during undrained shearing are illustrated in Fig. 3. The sample for this test was made by means of moist placement and consolidated under the normal stress of 196 kPa and shear stress of 0. After consolidation, the relative density reached 63.3% (1.15 in void ratio).

Figure 3a shows the variation of shear resistance and pore pressure in relation to shear displacement. To make a clear view on the generation of pore pressure accompanying the shear displacement in the initial period, a logarithmic abscissa of shear displacement within the range of 10 cm was taken, and thereafter linear abscissa was used to show that the test had been sheared to steady state (the point of **SSP** in Fig. 3a, for simplification, the steady state point will be termed as **SSP** in the followings), where the shear resistance did not reduce further more. As shown in this figure, immediately after the undrained shear stress was applied, shear displacement took

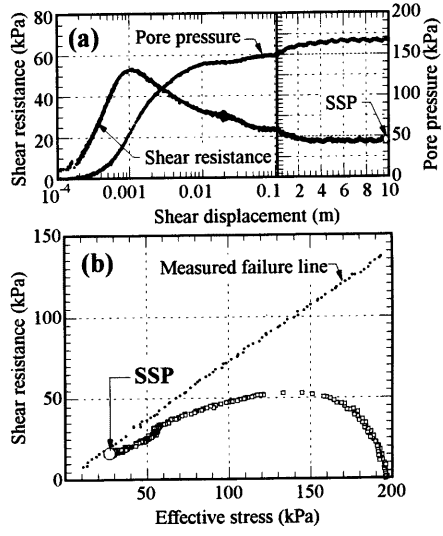

Fig. 3 Ring shear test on loose sand showing mass liquefaction phenomenon (B_D=0.99, D_r = 63.3%; SSP: Steady State Point). (a): Variation of pore pressure and shear resistance in relation to shear displacement; (b): Effective stress path.

place. Accompanying the increasing shear displacement, pore pressure built up quickly within limited shear displacement range (about 1 cm), and shear resistance decreased remarkably. This period is usually known as the collapse period, mainly due to the failure of metastable structure. After 3-cm shearing, accompanying the further increase of shear displacement, pore pressure built up gradually and then shear resistance decreased slowly as the subsequence. This process might be due to the grain crushing accompanying the shearing.

Figure 3b shows the effective stress path and failure line. The failure line was measured after the undrained shear test was stopped by means of unloading the normal stress at a very small rate while the low parts of ring shear apparatus was kept rotating at a constant speed under drained condition. From this figure, it could be seen that after undrained shear stress was added from 0.0, with increasing shear stress, stress path extended towards but did not reach the failure line until the final point, i.e., the steady state. This effective stress path showed the same changing tendency as that in undrained triaxial tests on loose sand. Therefore, it was treated as mass liquefaction in ring shear tests.

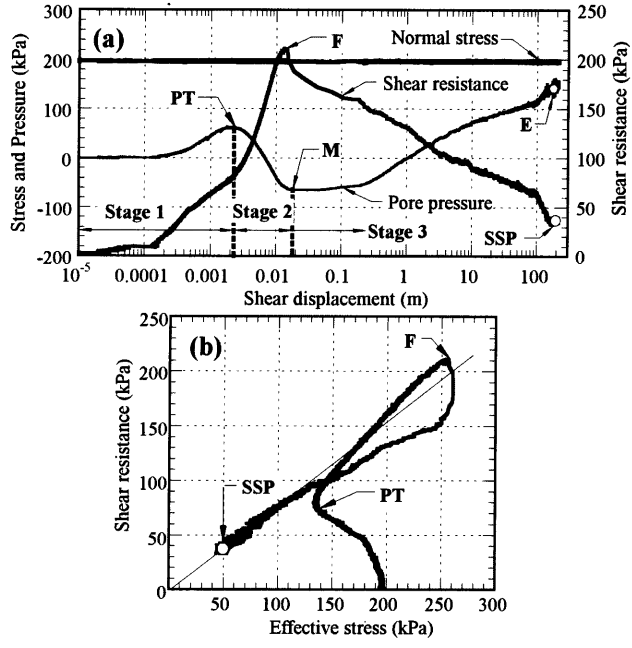

Fig. 4 Ring shear test on dense sand showing sliding surface liquefaction (B_D=0.99, D_r= 95.2%, σ = 196 kPa, PT: Phase Transformation; SSP: Steady State Point; F: Failure Point; E: Ending point). (a): Variation of pore pressure and shear resistance in relation to shear displacement; (b): Effective stress path.

Mass liquefaction appeared only in loose sand. Because all the tests were carried out under normally consolidated state, there were just limited tests showing mass liquefaction, while most of them showed another kind of fluidized failure of sliding surface liquefaction.

(2) Ring shear tests on medium to dense sand

Figure 4 shows the results of a test on dense sand of S8, in which appeared typical sliding surface liquefaction phenomenon. This sample was made by means of dry deposition with heavy tamping. After saturated and normally consolidated, the sample was sheared in undrained condition to a large displacement, 210 m. To shorten the rotating time after failure, in this test, torque control method with Medium gear (32.3 cm/sec) was selected. Fig. 4a illustrates the variation of pore pressure and shear resistance in relation to shear displacement; Fig. 4b shows the corresponding effective stress path. As shown in Fig. 4a, in the initial period after undrained shear stress was applied, with increasing shear displacement, pore pressure built up gradually. However, after point "**PT**", pore pressure decreased due to the dilatancy of dense sand. After the peak shear strength was reached (Point F in Figs. 4a, b), sample failed, and thereafter, pore pressure built up gradually with shear displacement, finally reached 145 kPa approximately. The shear resistance decreased slowly consequently, and finally fell to approximately 34 kPa. The excess pore pressure ratio, which is determined as the ratio of excess pore pressure and initial effective normal stress, was approximately 0.74. As shown in Fig. 4b, upon increase of shear stress, the effective stress path extended left-upward due to the pore pressure generation. After point "**PT**", the path went right-upward accompanying further shearing, showed a shape of "elbow" with a turn point. After failure point "F", the path fell downward along the failure line until a small shear stress. This is a typical stress path of sliding surface liquefaction.

According to Wang (1998), the pore pressure generation process along with the shear displacement could be divided into three stages as shown in Fig. 4a; **Stage 1**: from the beginning to point "**PT**" (where

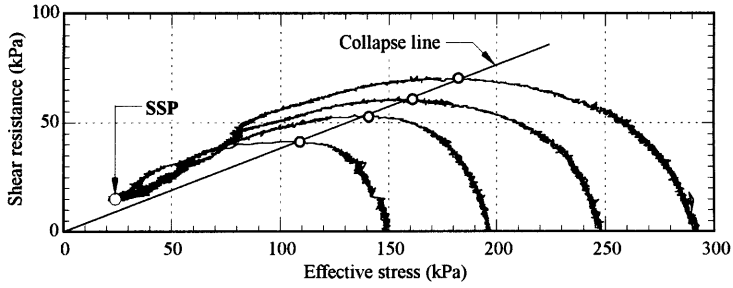

Fig.5 Results of tests on S8 at different initial normal stresses (D_r = 63.3%; SSP: Steady State Point).

the phase transformation was started, according to Ishihara, 1993), defined as the initial negative dilatancy area, it is mainly caused by the orientation of sand grains and the failure of metastable soil structure accompanying the increasing shear stress; **Stage 2**: from point "**PT**" to point "**M**" (where the pore pressure is the minimum), defined as initial positive dilatancy. With further increasing shear stress, sand grains adjust their positions, and/or move to each other. This would affect the adjacent particles significantly and lead to potential volume dilatancy, and then result in the reduction of generated pore pressure. **Stage 3**: form point "**M**" to final point "**E**" (means end of the shearing), defined as negative dilatancy due to grain crushing, which results in the potential volume shrinkage. Absolutely, the pore pressure generation in each stage depends on the initial state (including the initial relative density, normal stress, shear stress, shear history, and even the ageing of sample, etc.), and the characteristics of samples (including the grain size, fine-particle content, possibility of grain crushing, etc.).

The undrained shear behaviour in triaxial apparatus as that before the point "F" in Fig. 4b was described as limited liquefaction (Castro, 1969). Due to the limitation of triaxial apparatus in shear displacement, the behaviour after "F" was not obtained and not made clear until undrained ring shear apparatus was built and improved by Sassa and colleagues. Obviously, the prerequisite for this kind of liquefaction is that enough shear displacement could be offered for the effective happening of grain crushing.

In the liquefaction potential analysis based on triaxial test results, it has been pointed out that, for soil at a certain stress state, when the relative densities greater than those corresponding to the steady state line (obtained from undrained triaxial tests), the soil will exhibit dilative behaviour, and there will be no potential for liquefaction. However, the test results presented here shows that, provided that shear stress is great enough to initiate the failure of soil, liquefaction could be triggered, no matter the soil are in dense or loose state.

4.2 Effects of initial stress state

Fluidization landslides could be induced in different slopes, where the slope angle and soil depth may be different, i.e., the failure could be initiated at different initial stress state, and then the resulting failure could be different. To examine the effects of initial stress state on the fluidization landslides, in this test series, two sets of tests were conducted on S8 under different initial normal stresses and shear stresses respectively, and then the undrained shear behavior were examined.

It is worth to note here that, in these series tests, the void ratio (relative density) should be made the same, but due to the difficulties in making samples and the possible effects of different initial consolidation stress state, although efforts were made by performing numbers of tests and then selecting those results of tests with the void ratios being approximately the same, there are still little differences between the tests presented here in their initial relative densities. Considering the differences being very small, their effects are ignored in the following discussion.

(1) Effects of initial normal stress

Effects of initial normal stress on the undrained shear behaviour could be interpreted by Fig. 5, the effective stress paths for 4 tests on S8. The samples for these four tests were all made by means of moist placement. They were normally consolidated at initial normal stresses of approximate 147.0, 196.0, 245.0, and 294.0 kPa, respectively (corresponding to 1.5, 2.0, 2.5 and 3.0 kgf/cm^2, respectively), and then were all

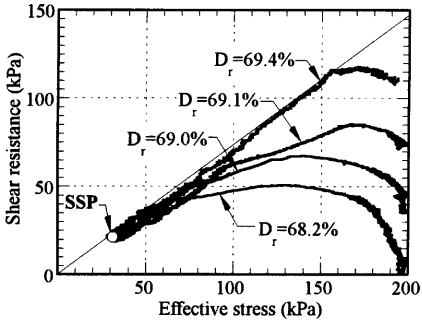

Fig. 6 Results of tests on S8 at different initial shear stresses (SSP: Steady State Point).

sheared to steady state by increasing the shear stresses from 0.0 at a loading rate of 0.098 kPa/sec (0.001 kgf/cm^2) under undrained condition. As exhibited in Fig. 5, with increasing initial normal stress, the peak strength becomes greater (peak shear strengths were 41.2, 54.1, 61.2, and 70.6 kPa, for the tests with normal stress being 147.0, 196.0, 245.0, and 294.0 kPa, respectively), showing a tendency that peak shear resistance increases with increasing initial normal stress. Nevertheless, the final point of each effective stress path tending to the same point shows that these four tests have the same steady state strength (approximate 15.0 kPa), irrespective of initial normal stresses. In this aspect, ring shear tests results showed a good consistency with those obtained from undrained triaxial tests, hollow-cylinder torsional shear tests, etc.

(2) Effects of initial shear stress

Four test results were plotted in Fig. 6 to interpret the effects of initial shear stress on the undrained shear behaviour of sand. The initial shear stresses for these four tests were 0.0, 34.5, 72.0, and 108.5 kPa, respectively, while the normal stresses were kept the same, 196.0 kPa. These four samples were all made by means of dry deposition without tamping, and were all normally consolidated.

Figure 6 shows the effective stress paths for these four tests. As shown, for each test, with increasing shear stress, the effective stress path tended leftward and finally reached the failure line, thereafter fell down along the failure line towards zero point. It is worth to pay attention to the fact that with increasing initial shear stress, the effective stress path reached to the failure line more quickly, and thereafter followed the failure line dropping towards zero point, as illustrated by the effective stress path of test at initial

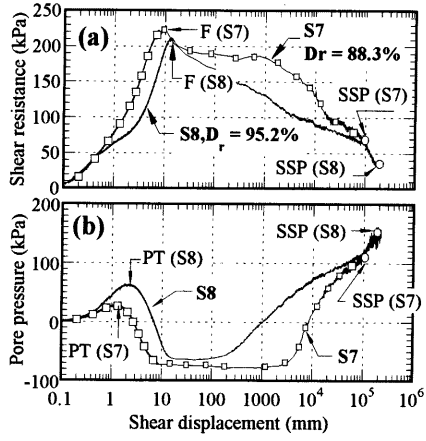

Fig. 7 Typical test results for dense S7 and S8.
(a): Shear resistance versus shear displacement;
(b): Pore pressures versus shear displacement.

shear stress of 108.5 kPa, which showed a typical sliding surface liquefaction behaviour.

From Figure 6, it could be seen also that with increasing initial shear stress, the peak shear strength become greater. Nevertheless, the final liquefaction resistances were approximately the same. The little differences between their values may be due to the little differences between their initial relative densities. As described above, denser sand will have greater steady state strength. Therefore, it could be concluded that initial shear stress has no influence on the steady state strength.

4.3 Effects of grain size

Here results of tests on sands in medium to dense state were selected to present the effects of grain size, and during comparison, relative density (D_r) was used to present their density. Because S7 and S8 are made from the same material (silica sandstone) through grinding method, it could be inferred that the differences between their undrained shear behaviors, if exist, are resulted from the different grain sizes.

Figure 7 presents the tests results of S7 and S8, illustrating the undrained shear behaviour of dense sands. The shear resistance-shear displacement curves (Fig.7a) and excess pore pressure-shear displacement curves (Fig. 7b) are typical and obtained from a series of tests. Theoretically, their relative densities should be made the same during comparison, but due to the difficulties in preparing the samples, the relative densities of the tests presented here are 88.3% for S7,

and 95.2% for S8. Nevertheless, the influence of grain size on the undrained shear behaviour could be seen evidently.

From Fig. 7a, it could be seen that before the peak shear strength was mobilized, the shear displacement at a certain shear stress is greater for S8, showed higher deformation potential than S7. And then the corresponding pore pressure builds up rapidly for S8 (see Fig. 7b). But after failure, S7 had a quicker increase in pore pressure accompanying the increasing shear displacement in the final period, as reflected evidently by the change in curvature of the pore pressure versus shear displacement plotted in Fig. 7b. And then the shear resistance decreases rapidly in the final period for S7 correspondingly. Usually, for the same sand, when relative density becomes greater, the generation of pore pressure along with shear displacement would become slower before the peak shear strength, and rapider after failure. Therefore, it could be concluded that the results illustrated in Fig. 7 were resulted from the influence of grain size. The difference could be interpreted by the main controlling factors in different shearing stages. For S7, its grain sizes are coarser; this makes the sand have less contacting points with greater average contacting forces acting on each of them. Therefore, it would be difficult for sand grains to orientate, and for the failure of metastable structure to happen in **Stage 1**. In **Stage 2**, the adjusting of position and motion of grains would result in higher dilatancy potential for coarser sand S7. During **Stage 3**, grain crushing happened in these coarser sands would result in higher potential of volume shrinkage, and then would result in quicker generation of pore pressure.

When we focus on the locations of phase transformation, peak shear strength and steady state in Figs. 7a, b, we can find that they are differing for S7 and S8. The corresponding peak shear stress and steady state for S7 are approximately 266, and 67 kPa, respectively; while those for S8 are 211, and 39 kPa, respectively, showing to be easier to suffer from liquefaction than S7.

4.4 Effects of fine-particle (loess) content

As aforementioned, although there are some inconsistencies between the research results of different researches, it was made clear that fine-particle (including its characteristics and its content) could affect the undrained shear behavior greatly. Therefore, in this test program, by changing the initial void ratio, series tests were conducted on each sample of M10, M20, and M30. In each test

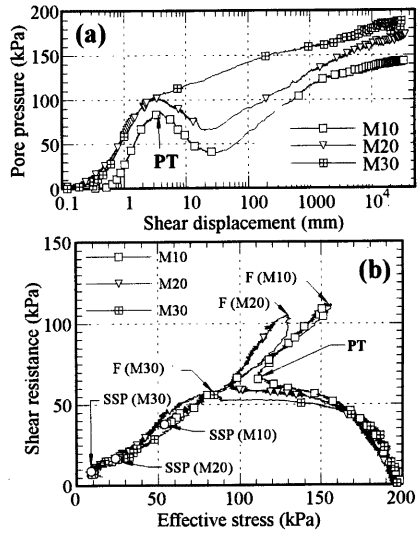

Fig. 8 Comparison on the results of tests on M10, M20, and M30 (PT: Phase transformation; Dr = 70.4%, 79.0%, and 80.5%, for M10, M20, and M30, respectively). (a): Variation of pore pressure along with shear displacement; (b): Effective stress paths.

series, when the initial relative density was different, the undrained shear behavior was differing, varying from mass liquefaction to sliding surface liquefaction. Here results of tests on medium to dense samples were selected also to illustrate the effects of fine-particle (loess) content on the undrained shear behavior. Because these samples with different loess contents were treated as different samples, here relative density was used when the comparison was made in this section, similar to the series tests described above.

Figures 8a, b show the results in the form of variation of pore pressure along with shear displacement and effective stress path, respectively, for the tests on dense M10, M20, and M30 with initial relative densities being 70.4%, 79.4%, and 80.5%, respectively (0.96, 0.89, and 0.89 in initial void ratio, respectively). As shown evidently, with increasing fine-particle content, the undrained shear behavior in the form of effective stress path changed remarkably. The test on dense M10 and M20 showed strong strain rehardening processes after the phase transformation point (**PT**), during which shear strengths increased greatly due to suction of dense samples, and after failure, shear strengths reduced accompanying the

generation of pore pressures. With increasing fine-particle (loess) content, this strain rehardening process becomes weaker, showing a reduction tendency in peak shear strength. For the test on dense M30, there was almost no rehardening process due to dilatancy. This tendency could be seen evidently from Fig. 8a, where the pore pressure generation along with shear displacement showed a continuous increase throughout the whole shearing process without any temporary reduction. Meanwhile, the steady state shear strength becomes smaller evidently with increasing fine-particle (loess) content. Therefore, It could be concluded that, with increasing fine-particle (loess) content (within the tested range of loess content, 30%), both the peak shear strength and steady state shear strength become smaller, i.e., become easier to suffer from liquefaction failure, while their initial relative densities are the same.

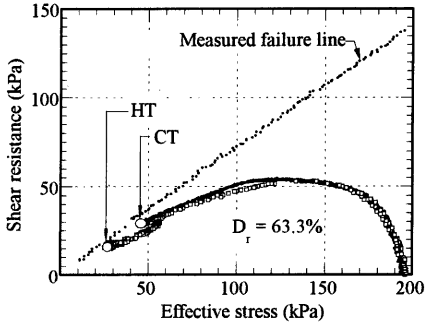

Fig. 9 Effective stress paths for the tests on loose sands (HT: host test; CT: complementary test; shear displacements are 10 m and 3 cm for HT and CT, respectively).

5. Mechanism of Fluidization in the Shear Zone

There are many investigations on the case studies showing that liquefaction was initiated within the sliding zone, and this zone might be a newly developed one due to shear failure, or the existed sand seam (or sand lenses) sandwiched in the soil layers (Castro et al. 1992; Seed 1968). It was widely known that the possibility that the shear zone might liquefy is determined by the initial condition of the sand, by the magnitude of the stresses induced by earthquake or some other triggers, by the initial stresses in the sand before the loading, and by the possibilities for dissipation of pore pressure in the shear zone as they build up during the loading. Although these understandings are very appealing and widely accepted, they were based on the experimental results of mostly triaxial tests. As has been pointed out, soil failure is often accompanied by the occurrence of localized deformation in thin zones of intense shearing. Therefore, using the global stress-strain measurements in triaxial apparatus would not be representative of the localized shear behaviour while localization formed within the specimen (Finno et al. 1996). Recently, there were some researches had been carried out to study the centralized liquefaction failure by means of shaking table (for example, Kokusho 1999), geo-centrifuge (Zeng and Arulanandan 1994), plane strain apparatus (Finno et al. 1996, 1997), etc.. However, due to the limitation of these apparatus in shear displacement, the grain crushing could not be complete, i.e., the ultimate steady state could not be reached. In this aspect, ring shear apparatus offered an available method.

5.1 Formation of localized fluidization in the shear zone

As mentioned previously, there are two kinds of different response in the undrained shear behaviors: mass liquefaction in loose state and sliding surface liquefaction in medium to dense state. To observe the shear behavior of sands in ring shear box, the shear deformation within the shear zone was observed after the two tests introduced in Figs. 3, 4 were finished. Meanwhile, to observe the deformation of the sand within the whole ring shear box, two complementary tests were conducted on S8, while keeping their relative densities being the same as those introduced in Figs. 3 and 4. In each of these complementary tests, two vertical 1-cm wide slices made from Toyoura standard sands, whose color differs obviously from that of S8, were made inside the samples. The samples were saturated and normally consolidated following the methods used in their host tests. After sheared to 3 cm in undrained condition, the tests were stopped. Thereafter, the upper parts of ring shear apparatus were removed and the deformation of the inserted slices were observed.

The undrained shear results of the complementary test on loose S8 (having the same relative density as that of the host test shown in Fig. 3) are presented in Fig. 9. To make a convenient comparison, results of the host test are presented also. As shown, within the shear displacement range of 3 cm, the complementary test and the host test behaved almost the same. Meanwhile, the pore pressure ratio reached approximately 0.75, indicating that a high excess pore

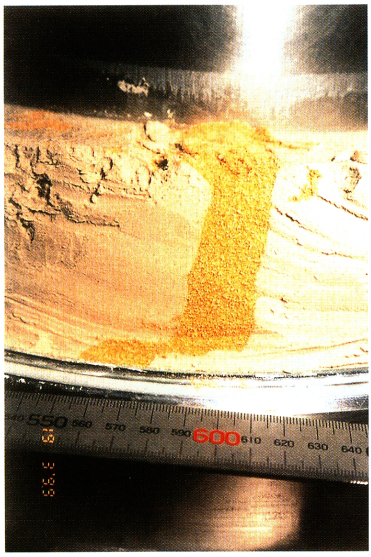

Fig. 10 Shear deformation of vertically inserted slice of Toyoura sand after 3-cm shear for the CT test shown in Fig. 9 (B_D = 0.99, Dr = 63.3%).

Fig. 11 Shear deformation of vertically inserted slice of Toyoura sand in the complementary test for the dense sand shown in Fig. 4 (B_D=0.99; D_r = 94.9%).

pressure has been resulted in at the place of shear displacement being 3 cm.

Figure 10 presents the shear deformation of one slice inside the shear box for the complementary test. The difference in color assisted in the identification of shear deformation. As shown in this photo, the upper part of the slice inclined slightly leftward to the shear direction due to the shear deformation within the upper part of sample. Nevertheless, there is no obvious disturbance within the slice, but a shear zone (approximately 0.5-cm thick) formed between the upper and low parts. Therefore, it could be concluded that the liquefaction is just localized in the shear zone. This shows a consistency with the result of test on sand by plane shear apparatus, with which, it is observed that shear banding could happen even in very loose sand (Finno *et al.* 1997).

The complementary test for observing the shear deformation in dense S8 showed that the slice stood nearly vertically even after sheared to 3 cm, and there was a very thin zone (even can not see the zone but a line in Fig. 11) formed between the upper and low parts, showing a highly centralized shearing along the shear zone.

5.2 Grain crushing within the fluidized shear zone

As stated by Sassa (1996), grain crushing plays the most important role in sliding surface liquefaction. Based on the tests results, Wang (1998) had performed an analysis on the relationship between grain crushing possibility of sand in dry state and the pore pressure generation in saturated condition when subjected to undrained shearing. However, the grain crushing in the undrained condition was less examined. Meanwhile, in the definition of steady state deformation proposed by Poulos (1981), it has been pointed out that steady state deformation could be reached only after the grain crushing, if existing, have finished. Therefore, the grain crushing was examined in the localized liquefaction phenomena of undrained ring shear tests.

First, the grain crushing analysis was performed on the test showing mass liquefaction (shown in Figure 3). After the test was finished, pore water was drained out from the shear box, by flowing air from the upper drainage hose and draining water from the lower drainage valve. By doing this, the sample could be kept relatively undisturbed, while moving the upper mechanical parts of the shear box away. Thereafter, samples were taken out from the shear zone. It should be noted that an annular shear zone showing allspice-shaped cross section was formed, which was differing from the upper and lower part in color evidently with extinguished interface between

(a)

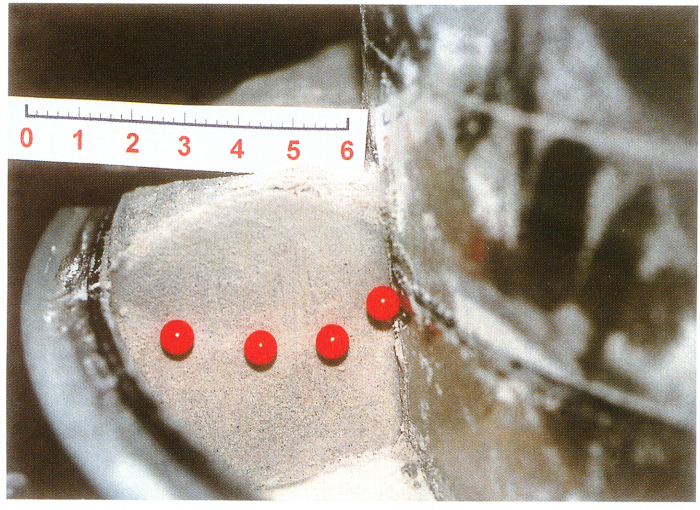

(b)

Fig. 12 Formation of shear zone for the tests on S8. (a): in loose state (D_r = 63.3%; Shear displacement = 10 m) ; (b): in dense state (D_r = 95.2%; Shear displacement = 210 m)

its upper and lower boundary (as shown in Fig. 12a). The grain size distributions of the original sample and that from the shear zone are illustrated in Fig. 13. Because the shear was carried out under undrained condition, and at the same time silica sand no. 8 is kind of fine sand with hard particles, the degree of grain crushing is not heavy. To make a clear view of the differences between each other, logarithmic ordinate was used in Fig. 13. As shown, the grain size distribution curve for the sample from shear zone is locating above that for the original sample, showing that grain crushing was initiated in the shear zone.

From Fig. 9, it could be seen clearly that after sheared to 3 cm, the sand showed a quick and great

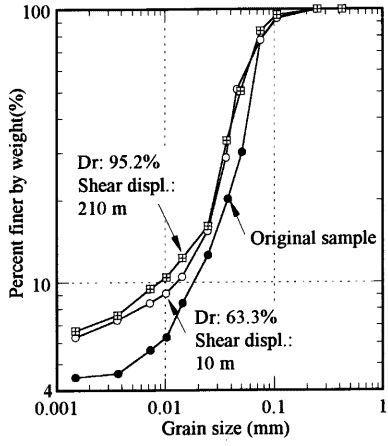

Fig. 13 Grain-size distribution of S8 after shearing.

loss in shear strength, and thereafter, the shear strength decreased slowly with increasing shear displacement. From the grain crushing analysis presented in Fig. 13, it could be considered that this slow reduction in shear strength was resulted from the grain crushing within the shear zone.

Following the same method, the grain crushing analysis was performed on the test of dense sample (presented in Fig. 4). The results are presented in Fig. 13, and it could be seen clearly that the sample from the shear zone is the finest, showing that more severe grain crushing happened in this test, due to longer shear displacement and greater density. It is needed to say that, after the test was finished and the upper parts of the shear box were moved, the shear zone was very clear, showing the same shape of cross section as, but thicker than, that in Fig. 12a (as shown in Fig. 12b).

From the cross section of the shear zone appeared in both the loose state and dense state, it could be inferred that the shear was localized in the shear zone, no matter whether the sand was in loose state or in dense state. Therefore, it could be concluded that liquefaction was limited in the shear zone in ring shear tests.

5.3 Collapse behaviour of loose sand within the shear zone

To analyze the undrained shear behavior of loose sand, the collapse behaviors in ring shear tests at different initial normal stresses were examined. As reflected by Fig. 5, the point of peak shear strength at each effective stress path lies on the same line, which was referred to as "collapse line" by Sladen (1985). According to Sladen's proposition, this line binding the points of peak shear strengths for the tests at different normal stresses passes through the steady state point, and is dependent on initial void ratio. Similar to this concept of collapse line, Vaid and Chern (1983) proposed a concept of "critical stress ratio line" (CSR), and they found that the points of peak shear strengths lie in the same line, and this line projects back through the origin and is independent on initial void ratio. This CSR line is called the flow liquefaction surface (FLS), presenting the onset of flow liquefaction. It could be seen that these two concepts of collapse line and critical stress ratio line share the same meaning: marking the onset of quick strain softening that would result in flow liquefaction. Nevertheless, they showed controversies evidently, although they were all based on triaxial compression tests results. Some commenced research works support Sladen's collapse line (Ishihara 1993; Sasitharan et al. 1994). Meanwhile, "Critical stress ratio line" was supported also by some studies (Vaid *et al.*1989; Alarcon-Guzman *et al.* 1988; Negussey *et al.* 1988; Konrad 1993). In this undrained ring shear tests, from the tendency of collapse line drawn in Fig. 5, it could be seen evidently that collapse line projects back through origin.

As aforementioned, the grain size could affect the undrained shear behavior. To examine the effect of grain size on the collapse behavior, here a series of tests was conducted on S7 at different initial normal stresses. The results of tests on loose S7 were presented in Fig. 14a. From this figure, it could be found easily that collapse behaviour happened in each test: after the peak shear strength was mobilized, the sand failed rapidly accompanying the quick generation of pore pressure and reduction in shear resistance; connecting the peak strength points formed a collapse line and this collapse line projected back trough the origin. A comparison of the inclination of collapse line shown in Fig. 5 and that shown in Fig. 14a could result in a finding that the collapse line for loose S8 in Fig. 5 is steeper than that for S7 in Fig. 14a. This could be interpreted by the different relative densities. As shown above, in these series tests, although the void ratios in series tests on S8 were approximately 1.15, while those in the series tests on S7 were approximately 0.98, seemed denser than S8, the relative densities for the series tests on S8 were approximately 63.3%, while those for the series tests on S7 were approximately 47.2%, evidently smaller than that of the tests on S8.

To compare the effects of grain size on collapse

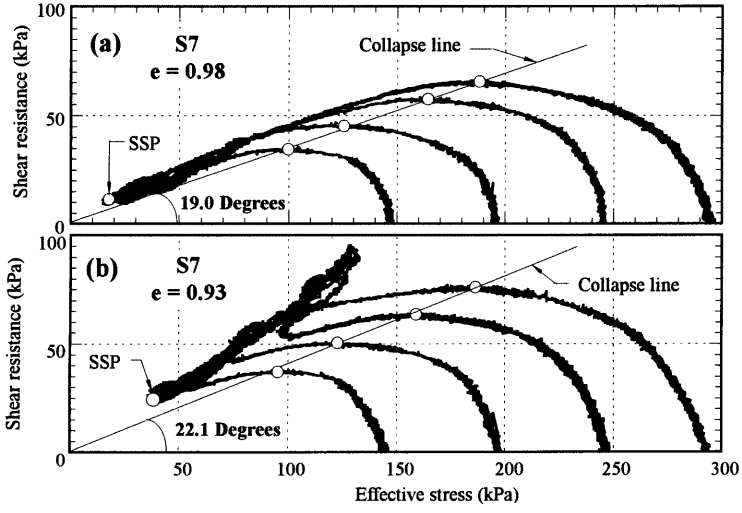

Fig. 14 Effective stress paths for the tests on loose S7 at different initial normal stresses. (a), (b): for the tests with D_r being approximately 47.2% and 56.6%, respectively.

behavior, it is desirable to conduct the tests on S7 and S8 at the same relative densities. However, as proved by the results of a trial test on S7, when the initial relative density reached at 57.9%, the undrained shear behavior showed a typical sliding surface liquefaction phenomenon with a strong rehardening process, namely without any collapse behaviour that could result in the quick liquefaction failure. Hence, it could be inferred that when the relative density of S7 reaches 63.3%, at which S8 showed quick collapse failure, there would be no collapse failure behavior for S7. Nevertheless, a series of trial tests on S7 with collapse behavior in the undrained shear process showed that collapse behaviour is dependent on the grain size as well as on the relative density. The samples of this series tests were made by means of dry deposition without tamping and consolidated at different normal stresses with void ratios being approximately the same, 0.93 (56.6% in relative density). The tests results were presented in Fig. 14b in the form of effective stress path. As shown, in each test, after the peak strength (before the re-hardening process) was mobilized, the sample failed, showing an evident collapse process during which excess pore pressure generated quickly and shear resistance reduced consequently. However, after a certain period of quick strain-softening, the sand re-hardened, and showed a limited increase (very small) in shear resistance before the failure; after failure, with increasing shear displacement, pore pressure built up and then shear resistance was reduced consequently, this led to the effective stress path dropped down along the failure line. It could be seen that the final point of each test tended to approximately the same value, and binding the peak strength (before the re-hardening process) of each test formed a direct line that projects back the origin, showing consistency with the tests results of those two series described above. Comparing this collapse line with that of S8 shown in Fig. 5 could lead to a finding that the collapse line for S7 at relative density of 56.6% is steeper than that for S8 at the relative density of 63.3%. Meanwhile, as shown, the inclination of the collapse line in Fig. 14a is approximately 19.0 degrees, while that in Fig. 14b is approximately 22.1 degrees. Although the difference in inclination is just two degrees, considering the difference between their void ratios is very small (just 0.05 in *e* value), it could be seen that the increase tendency of inclination of collapse line with initial void ratio is evident. Therefore, it could be concluded that the collapse behavior was affected not only by the grain size, but also by the initial relative density.

5.4 Brittleness index for sand at different stress states

The reduction in soil shear strength resulted from

the initiation of liquefaction may be large or small, and it may depend on the initial void ratio, stress state and shear history. The magnitude of the strength loss after initiation of liquefaction does not directly affect the safety against initiation of liquefaction, but it has a large effect on the consequences of liquefaction. After liquefaction has been initiated in an element of soil, that element accelerates to deform until it reaches the steady state of deformation. In this process, the shear resistance drops from the peak shear strength to the residual (steady state in most situation) shear strength. To analyze the post-rupture behaviour, Bishop (1967) proposed a parameter "Brittleness index" to express the reduction in undrained strength of a strain-softening material, which was defined as:

$$I_B = (\tau_f - \tau_r)/\tau_f \quad \text{.....(2.2)}$$

Where τ_f is the peak shear strength, and τ_r is the residual undrained shear strength, namely the steady-state shear strength in many undrained shear tests. A greater brittleness index indicates a greater reduction in shear strength that means progressive development of large deformation could be resulted in after the initiation of liquefaction.

From field observations, it is normally understood that slope failure behavior is controlled by the slope angle and soil thickness, namely well connected with the initial stress state. To predict the fluidized slope failure behaviour through the tests results, here the brittleness index was used to examine the fluidization behavior after failure. Because the brittleness index is strongly dependent on the initial density, to minimize the effects of initial density, here the effects of stress state on the brittleness index will be examined basing on those tests presented in Figs. 5 and 6.

The effect of initial normal stress on the brittleness index could be seen evidently from an observation on Fig. 5, where the undrained peak shear strength increases with increasing initial normal stress, while the steady state shear strengths for all the tests are approximately the same. Therefore, it could be concluded that the brittleness indexes are differing from each other (I_B = 0.64, 0.72, 0.75, and 0.79, for the test with normal stress being 147.0, 196.0, 245.0, and 294.0 kPa, respectively), and the test on sand consolidated to greater normal stress has a greater brittleness index, just as shown in Fig. 15a. Therefore, it could be inferred that for a fluidized landslide in practice situation, the thicker the failed soil mass is, the faster and longer the soil mass would move.

The effect of initial shear stress on brittleness index could be drawn also from Fig. 6, through which

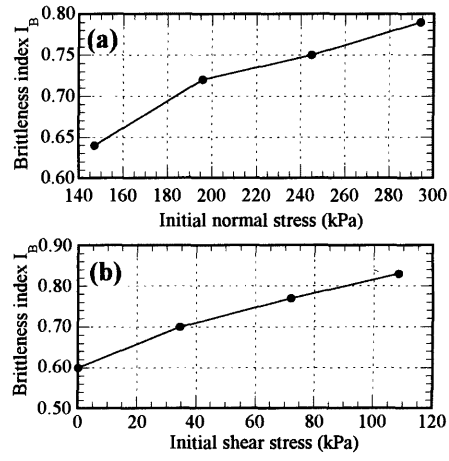

Fig. 15 Brittleness indexes at different initial stress states. (a) at different initial normal stresses; (b) at different initial shear stresses.

it could be seen that the peak shear strength becomes greater with increase of initial shear stress while the steady state shear strength is the same. Therefore, the brittleness index (I_B) becomes greater consequently. This tendency is illustrated evidently in Fig. 15b, where the brittleness indexes are plotted against initial shear stresses. Therefore, It could be concluded that the fluidized landslide initiated at a steeper slope will suffer from faster and larger progressive motion.

5.5 Characterization of fluidization behavior of sand with different grain size and fine-particle (loess) contents

In dealing with the possible fluidization behavior of a soil mass in the field, the pore pressure generation process, peak shear strength and steady state strength may be the key parameters. Therefore, the different characterization of fluidization behavior of sands due to the change in grain size and fine-particle (loess) content will be examined in these three aspects.

(1) Pore pressure generation at different stages

As mentioned before, mass liquefaction only appeared in loose sand, while most of them showed sliding surface liquefaction, where a process of *negative dilatancy–positive dilatancy–negative dilatancy* appeared with the increasing shear displacement (described as Stage 1 to Stage 3 in Fig. 4), therefore, to examine the effects of grain size on the compressibility, dilatability and crushing

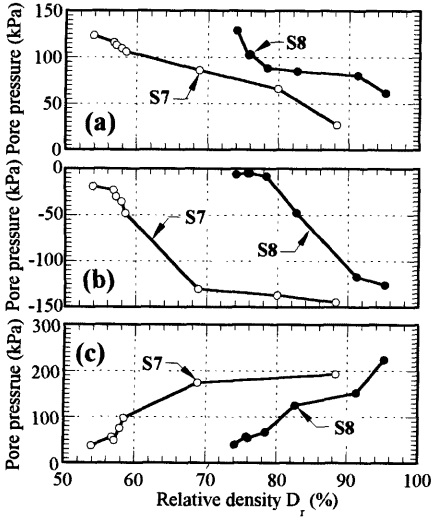

Fig. 16 Generated pore pressure against relative density during different undrained shear periods. (a): period before phase transformation; (b): period after phase transformation but before failure; (c): period after failure.

characteristic of samples respectively, the effects of grain size on pore pressure generation during these different stages (for sliding surface liquefaction) were examined. In the present stage of this research, tests were conducted on S7, S8, M10, M20, and M30, respectively, namely on samples with grain size becoming finer. Because there was no rehardening process for the tests on M30, here the results of tests on S7 and S8 are used to illustrate the effects of grain size on the pore pressure generation.

The pore pressures generated in different stages (shown in Fig. 4) were examined separately for the tests on S7 and S8, and plotted in Fig. 16 against relative density. Fig. 16a reflects the generated pore pressure due to shear deformation before the phase transformation point, corresponding to **stage 1**. As showing, S8 has a greater pore pressure than S7 at this stage, while their relative densities are the same. This substantiates the explanation given previously, finer sand S8 having higher deformation potential than S7. Fig. 16b presents the reduction of pore pressure due to dilatancy of dense sands, corresponding to **Stage 2**. It could be seen that the generated pore pressures were all negative during this period. From the fact that the reduction of pore pressure for S7 is greater than that for S8, while their relative densities being the same, it could be

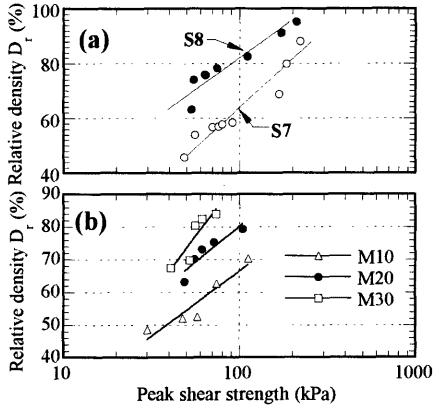

Fig. 17 Peak shear strength against D_r. (a): For the tests on S7 and S8; (b): For the tests on M10, M20, and M30.

concluded that dense coarser sand has greater dilatancy potential when subjected to undrained shearing. But when we focus on Fig. 16c, we could find that the initiated pore pressure for S7 in **Stage 3** is greater than that for S8, showing that coarser sand has higher volume shrinkage potential due to grain crushing during shearing.

(2) Undrained peak shear strength

For the tests carried out under the same initial stress state, the peak shear strength could reflect whether it is difficult for a given sample to suffer fluidization failure or not. Therefore, emphasis was directed to the peak shear strength during the analysis of fluidization behaviors of sands with different grain size and fine-particle (loess) contents.

Because the peak shear strength is dependent on the initial stress state, here the peak shear strengths are all those tests carried out under the same initial stress state (initial normal stress = 196 kPa, and initial shear stress = 0). The peak shear strengths versus relative density for S7 and S8 are plotted in Fig. 17a. An observation of this figure could immediately lead to an understanding that S7 has a greater peak shear strength than S8, while their relative density are provided the same.

The peak shear strength for M10, M20, and M30 were plotted in Fig. 17b against relative density. As reflected in this figure, peak shear strength increases with increasing relative density for each sample. From the changing trend of each sample, it could be seen that given the initial relative density being the same, the peak shear strength becomes smaller with

increasing fine-particle (loess) content (within the tested range of loess content of 30%).

From the tests results presented above, it could be concluded that when the grain size becomes finer or with increasing fine-particle (loess) content (within tested loess content limitation of 30%), the sample becomes easier to suffer fluidization failure.

(3) Steady state strength

Steady state strength plays an important role in the motion of fluidized soil mass. It is directly related to the final slope angle when the fluidized mass stopped. As an important component in analyzing the fluidization behavior of sands with different grain size and fine-particle (loess) contents, here the steady state strengths are examined.

Although the steady state strength is just a function of initial relative density, irrespective of initial stress state, the apparent friction angle for a test (Sassa, 1985) is dependent on the initial normal stress. To analyze the fluidization behavior of sample, here those strengths at steady state for all the samples are from all the tests conducted at different initial void ratios and the same initial normal stress (196 kPa).

Figure 18a show the steady state points for S7 and S8, plotted on a D_r versus log(τ_s) plane, where τ_s is the shear strength at steady state. From the tendency, it could be seen that the steady state line of S8 is located above that of S7, showing that finer sand S8 has smaller shear strength than S7, while their relative densities being the same.

The steady state strengths for M10, M20, and M30 were presented in Fig. 18b also, in the form of shear strength against relative density. As shown, with increasing fine-particle (loess) content, the steady state line shifts the position from that of the M10; when the relative density for each of them are the same, the shear strength at steady state becomes smaller with increasing fine-particle (loess) content, at least within the range of loess content being 30%.

According to the observation on many fluidized landslides where the apparent friction angles were not greater than 10 degrees, here a criterion for judging the initiation of fluidization was given as that the apparent friction angle is less than 10 degrees, namely the undrained shear strength at steady state should be less than 34.6 kPa in the undrained ring shear tests, given the initial normal stress being 196 kPa (Wang 1999). Here we use τ_c to term this value of 34.6 kPa. The corresponding line is drawn in Fig. 18 in the form of dotted line, and then the area on the left of this line presents that fluidization is initiated, while the area on the right presents no fluidization.

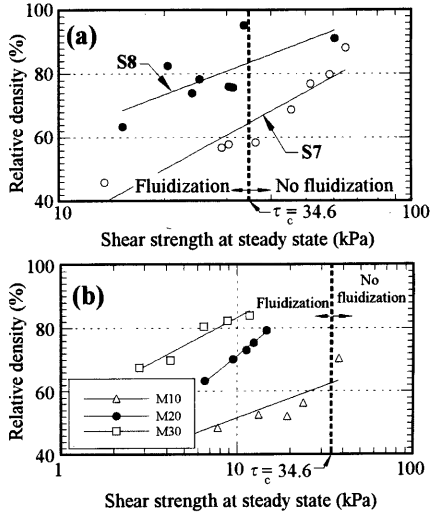

Fig. 18 Shear strength at steady state against D_r. (a): For the tests on S7 and S8; (b): For the tests on M10, M20, and M30.

Therefore, the relative density (D_{rc}) corresponding to that at the intersection point of the steady state line and this dotted line for each sample is critical; when the initial relative density is smaller than this value, fluidization could be initiated, while greater, no fluidization. From Fig. 18a, it could be seen that this value of D_{rc} for S8 is much greater than that for S7. Meanwhile, Fig. 18b shows the same tendency: with increasing fine-particle (loess) content, this value of D_{rc} is becoming greater, and the when the fine-particle (loess) content increases to some extent (30% of loess content), fluidization could be initiated in almost all the tests, even in the most dense state.

5.6 Maintaining of generated pore pressure in shear zone

In practice situation, there were many cases where liquefaction had been initiated but the liquefaction-induced movements were of only limited extent (Seed 1968). Although there are many reasons why a slide caused by soil liquefaction may not result in large deformations, the maintaining of generated pore pressure may be the most important factor. Liquefaction can only persist as long as high pore pressures persist in a soil; if drainage can occur rapidly then liquefaction may persist for such a short period of time that large displacements are unable to develop. In practice, the liquefied soil mass could be

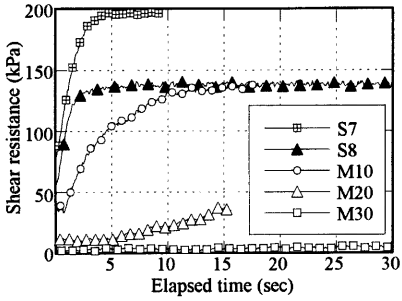

Fig. 19 Recovering of shear resistance due to excess pore pressure dissipation from the shear zone.

regarded as in undrained conditions during the very short period of failure triggered by earthquake, rainfall or some other factors, but could not be treated as in undrained condition throughout the whole moving process. Therefore, the persisting of generated pore pressure will be an important factor affecting the run-out distance of a fluidized landslide in the field, just as stated by Seed (1968). Considering that in this ring shear test series and in many historic liquefaction failures, liquefaction was limited in the shear/slide zone, it is highly desirable to have an insight into the maintaining of pore pressure in the shear zone. Therefore, a series ring shear tests was carried out to examine the dissipation of generated pore pressure in the shear zone. During tests, the saturated samples were shear in undrained condition to a large displacement where the liquefaction was ensured to have been initiated, and thereafter turned the shear box into drained condition to observe the dissipation of generated pore pressure and recovering of the shear strength.

Figure 19 presents the results of tests on S7, S8, M10, M20, and M30, where the shear resistances are plotted against the elapsed time. In all these tests, the moment when the shear box was turned into drained condition was treated as the zero point of elapsed time. Because the recorded value in pore pressure transducers just present the pore pressure outside the shear zone, when the shear box turned into drained condition, the pore pressure within the shear zone could not be observed correctly. Nevertheless, the recovering of shear strengths could reflect the dissipation of generated pore pressure. As shown in Fig. 19, when the shear box was turned into drained condition, the shear strengths of S7, S8, M10, M20 were recovering with the elapsed time, i.e., with the dissipation of generated pore pressure. However, an observation on the inclination of each curve (recovering rate of shear strength) could direct to the finding that the when the sample became fine and the fine-particle (loess) content became greater, this recovering rate of shear strength was becoming smaller, especially for the test on M30, there was almost no recovering tendency could be seen. Therefore, it could be inferred that once the liquefaction was initiated in the soil mass containing greater fine-particle, the pore pressure could be kept for a long time that would result in large deformation. This result showed a consistency with many laboratory researches and field cases (Seed 1968; Zeng and Arulanandan 1995).

6. Summary and Conclusions

Several sets of undrained ring shear tests were conducted on S7, S8 and the mixtures of S8 with different loess content to study the fluidization behavior of the shear zone. Based on the tests results, the effects of initial relative density, initial normal stress, and samples on the undrained shear behavior were examined. The conclusions could be drawn as follows.

(1) Mass liquefaction could only happen in loose sands, while sliding surface liquefaction could take place even in medium or dense sands. Both mass liquefaction and sliding surface liquefaction are limited in the shear zone, and grain crushing existed in both of them.

(2) Examination on the collapse behaviour of loose sand shows that ring shear tests results are in support of Sladen's assumption that collapse line is dependent on initial void ratio, but the collapse line in ring shear test tends much more to pass through origin, not through the steady state point.

(3) Grain size plays an important role in the undrained shear behaviour. Finer sand has smaller peak shear strength and steady state strength than coarser sand while their relative densities are the same.

(4) With increasing fine-particle content in the mixture, both the peak shear strength and steady state shear strength decrease. Meanwhile, tests on dense mixtures show that there is almost no re-hardening process in shear strength in the mixture with loess content being 30%, even though in dense state.

(5) When the grain size becomes finer and fine-particle content becomes greater, the dissipation of generated pore pressure within the shear zone becomes slower when turned into drained condition.

Acknowledgements

The authors wish to thank Dr. Hiroshi Fukuoka, assistant professor of Disaster Prevention Research Institute, Kyoto University, and Dr. Fawu Wang, Researcher of Center of Excellence at Kyoto University, for their suggestions and discussions throughout this research.

References

Alarcon-Guzman, A., Leonards, G. A. and Chameau, J. L. (1988). Undrained monotonic and cyclic strength of sands. *J. Geotech. Engrg., ASCE.* 103(10), 1089-1110.

Anderson, S. A., and Sitar, N. (1995). Analysis of Rainfall-Induced Debris Flow. *J. Geotech. Engrg., ASCE.* 121(7), 544-552.

Bishop, A.W. 1969. Progressive failure-with special reference to the mechanism causing it. *Proc. Geotech. Conf.*, Oslo, Norway 2, 142-150.

Bishop, A.W. (1973). The stability of tips and spoil heaps. *Q.J. Engrg. Geol.* 6, 335-376.

Bromhead, E. N. (1979). A simple ring shear apparatus. *Ground Engineering*, Vol. 12, No. 5, pp. 40-44.

Casagrande, A. (1971). On liquefaction phenomenon. *Géotechnique* 21, No. 3, 197-202.

Casagrande, A. (1976). Liquefaction and cyclic mobility of sands-a critical review. *Harvard Soil Mechanics Series.* 88.

Castro, G. (1969). *Liquefaction of sands.* Ph.D. Thesis, Harvard University, Cambridge, Massachusetts.

Castro, G., Seed, R. B., Keller, T. O., and Seed, H. B. (1992). Steady-state strength analysis of Lower San Fernando Dam slide. *Journal of Geotechnical Engineering*, ASCE, 118(3), 406-427.

Castro, G. & Poulos, S.J. (1977). Factors affecting liquefaction and cyclic mobility. *J. Geotech. Engrg. Div., ASCE.* 103, 501-516.

Eckersley, J. D. (1985): Flowslides in stockpiled coal. *Engrg Geol.* 22, 13-22.

Eckersley, J. D. (1990). Instrumented Laboratory Flowslides. *Géotechnique* 40, No. 3, 489-502.

Finn, W.D.L. (1981). Liquefaction potential: developments since 1976. *Proc., 1st International Conference on Recent Advances in Geotechnical Earthquake Engineering and Soil Dynamics*, St. Louis, 2, 655-681.

Finno, R.J., Harris, W.W., Mooney, M.A., and Viggiani, G. (1996). Strain Localization and Undrained Steady State of Sand, *Journal of Geotechnical Engineering*, ASCE, Vol. 122, No. 6, pp. 462-473.

Finno, R. J., W. W. Harris, M. A. Mooney and Viggiani, G. (1997). Shear bands in plane strain compression of loose sand. *Géotechnique* 47, No. 1, 149-165.

Georgiannou, V. N., Burland, J. B. & Hight, D., W. (1990). The undrained behaviour of clayey sands in triaxial compression and extension. *Géotechnique* 40, No. 3, 3431-449.

Guo Tianqiang & Shamsher Prakash. (1999). Liquefaction of silts and silt-clay mixtures. Journal of Geotechnical and Geoenvironmental Engineering, ASCE, Vol. 125, No. 8, pp. 706-710.

Ishihara, K. (1993). Liquefaction and flow failure during earthquakes. *Géotechnique* 43, No. 3, 349-451.

Ishihara, K. (1985). Stability of natural deposits during earthquakes. *Proc. 11th Int. Conf. Soil Mech.*, San Francisco, 1, 321-376

Ishihara, K., Okusa, S., Oyagi, N., & Ischuk, A. (1990). Liquefaction-induced flowslide in the collapsible loess deposit in Soviet Tajik. *Soils and Foundations* 30, No. 4, 73-89.

Kokusho, T. (1999). Water film in liquefaction sand and its effect on lateral spread. *Journal of Geotechnical and Geoenvironmental Engineering*, ASCE, Vol.125, No. 10, pp.817-826.

Konrad, J. M. (1993). Undrained response of loosely compacted sands during monotonic and cyclic compression test. *Géotechnique* 43, No. 1, 69-89.

Kramer, K. L. & H. B. Seed (1988). Initiation of soil liquefaction under static loading conditions. *J. Geotech. Engrg.*, 114: 412-430.

Marui, H. (1996). Preliminary report on the Gamahara torrent debris flow of 6 December 1996, Japan. *Jour. Natural Disaster Science.* 18, 89-97.

Negussey, D., Wijewickreme, W. K. D., and Vaid, Y. P. (1988). Constant volume friction angle of granular materials. *Can. Geotech. J.* Vol. 25, pp. 50-55.

OVANDO-SHELLEY, E., and B. E. PEREZ. (1997). Undrained behaviour of clayey sands in load controlled triaxial tests. *Géotechnique* 47, No. 1, 97-111.

Poulos, S. J. (1981). The steady state of deformation. *J. Geotech. Engng Div. ASCE* 107, No. GT5, 553-562.

Poulos, S. J., Castro, G. & France, J. W. (1985). Liquefaction evaluation procedure. *J. Geotech. Engng. Div. ASCE* 111, No. 6, 772-792.

Sasitharan, S., Robertson, P. K., Sego, D. C., and Morgenstern, N. R. (1994). State-boundary surface for very loose sand and its practical implications.

Can. Geotech. J. Vol. 31, pp. 321-334.

Sassa, K. (1985). The mechanism of debris flows. *Proc., XI Int'l. Conf. Soil Mech. Found. Engrg.*, San Francisco, 3, 1173-1176.

Sassa, K. (1988a). *Motion of Landslides and Debris Flows-Prediction of hazard area-*. Report for Grant-in-Aid for Scientific Research by Japanese Ministry on Education, Science and Culture (Project No. 61480062), pp.15.

Sassa, K. (1996). Prediction of earthquake induced landslides. Special Lecture of 7th International Symposium on Landslides, "*Landslides*", Rotterdam: Balkema, 1, 115-132.

Sassa, K. (1997). A new intelligent type of dynamic loading ring-shear apparatus. *Landslide News*. No.10, pp.33.

Sassa, K., H. Fukuoka, and F. W. Wang. (1997a). A geotechnical simulation test on the Gamahara torrent debris flow with ring shear apparatus (in Japanese). *Journal of the Earth*, Vol.19, No.10, pp.645-651.

Sassa, K., Fukuoka, H. and Wang, F. W. (1997b). Mechanism and risk assessment of landslide-triggered-debris flows: Lesson from the 1996.12.6 Otari debris flow disaster, Nagano, Japan. Landslide Risk Assessment (ed. Cruden and Fell), *Proceedings of the Int'l Workshop on Landslide Risk Assessment*, 347-356. Rotterdam: Balkema.

Sassa, K., Fukuoka, H. and Wang, F. W. (1998). Mechanism of Rapid Long Runout Motion in the may 1997 Sumikawa Reactivated Landslide in Akita Prefecture and the July 1997 Harihara Landslide-Debris Flow, Kagoshima Prefecture, Japan. *Journal of Japan Landslide Society*, Vol. 32, no. 2, pp. 29-37.

Seed, H. B. (1966). A Method for Earthquake Resistant Design of Earth Dams. *J. Geotech. Engrg Div. ASCE*, Vol. 92, No. SM1, Proc. Paper 4616, pp. 13-41.

Seed, H.B. (1968). Landslides during earthquakes due to soil liquefaction. *Journal Soil Mechanics Foundations Division, ASCE*, 94, No. 5, 1055-1122.

Seed, H. B. (1979). Soil liquefaction and cyclic mobility evaluation for level ground during earthquakes. *J. Geotech. Engrg Div. ASCE*, 105, 201-255.

Turner, A. K., and Schuster, R. L. (1996). Landslides: Investigation and mitigation. National academy press, Washington, D. C.

Vaid, Y. P., and Chern, J. C. (1983). Effects of static shear on resistance to liquefaction. *Soils and Foundations*, Vol. 23, No. 1, pp. 47-60.

Vaid, Y. P., Chung, E. K. F., and Kuerbis, R. H. (1989). Stress path and steady state. *Can. Geotech. J.* Vol. 27, pp. 1-7.

Vankov D.A., and Sassa, K. (1998). Dynamic testing of soils by ring-shear apparatus. *Proc. 8th Congr. of the Int'l Assoc. Engrg. Geol. and the Environ.*, Vancouver, Canada. Rotterdam: Balkema, Vol.1, pp485-492.

Wang, F. W. 1998. An experimental study on grain crushing and excess pore pressure generation during-shearing of sandy soils-A key factor for rapid landslide motion. PhD Thesis. Kyoto University.

Wang, Gonghui. 1999. An experimental study on the mechanism of fluidized landslide – with particular reference to the effect of grain size and fine-particle content on the fluidization behavior of sands. PhD Thesis. Kyoto University.

Yoshimi, Y., Richart, F.E., Prakash, S., Balkan, D. D. & Ilyichev, V. A. (1977). Soil dynamics and its application to foundation engineering. *Proc., 9th Int. Conf. Soil Mech.* 2, 605-650.

Zeng, X. and Arulanandan, K. "Modeling the Lateral Sliding of a Slope due to Liquefaction of a Sand layer," *Journal of Geotechnical Engineering*, ASCE, Vol. 121, No.11, 814-817, 1995.

要旨

土砂の流動化のメカニズムを調べるために、硅砂及び硅砂とレスの混合サンプルを用いてﾘﾝｸﾞせん断試験を実施した。その結果、非排水状態において、せん断ゾーンが形成しうることと粒子破砕はせん断ゾーンにおいて発生することが分かった。粗な試料には構造破壊（Collapse）によって流動化するが、より密度の大きな場合でもせん断の進行とともに流動化が発生し得る。ピーク強度と流動化後の強度の差とピーク強度の比（Brittleness Index）は初期応力状態の影響が強い。また、ピークせん断強度と流動限界勾配を規定する流動化後の定常状態強度は、粒径が小さい場合ほど細粒部分の比率が高いほど小さくなる。

キーワード：非排水挙動、過剰間隙水圧、せん断抵抗、リングせん断試験、粒径、細粒分含有量